Four Radionuclide Methods for Left Ventricular Volume Determination: Comparison of a Manual and an Automated Technique

Wayne C. Levy, Manuel D. Cerqueira, Dale T. Matsuoka, George D. Harp, Florence H. Sheehan, and John R. Stratton

Division of Cardiology, Department of Medicine and Division of Nuclear Medicine, Department of Radiology, Seattle Veterans Affairs Medical Center and the University of Washington, Seattle, Washington

This study compared the accuracy and reproducibility of three previously described and one new radionuclide method of measuring left ventricular volumes in 19 subjects using contrast ventriculographic volumes (n = 38, mean volume = 126.6 ml) as the gold standard. The four methods were compared using both manual and automated ROIs. For manual ROIs, the Links (189.7 ml, r = 0.85), Starling (183.2 ml, r = 0.77) and the new count ratio method (141.4 ml, r = 0.90) overestimated contrast volumes, while the Massardo method (122.5 ml, r = 0.91) provided accurate volumes. For the automated ROIs, we performed an interpolative background subtraction and used a 50% threshold of the highest count pixel to define the ventricular regions. The automated Massardo method severely underestimated the contrast volume (59.5 ml, r = 0.90), while the other automated methods yielded accurate volumes: Links (122.4 ml, r = 0.89), Starling (118.1 ml, r = 0.81) and the new count ratio method (125.0 ml, r = 0.90). The interobserver reproducibility of the automated methods was excellent (mean difference = 1%–4%) compared to the manual methods (2%–8%). Because no additional images, blood counting, attenuation, or decay correction were necessary, the manual Massardo method and the automated count ratio method are the simplest to perform. We conclude that automated determination of left ventricular volumes using the new count ratio method is rapid, accurate, reproducible and could readily be incorporated into routine clinical use.

J Nucl Med 1992; 33:763–770

Ventricular volumes can be measured by contrast angiography, echocardiography and planar (*1–5*) and single-photon emission computed tomographic radionuclide angiography (*6–8*). Although radionuclide imaging is widely used for evaluating ventricular function and regional wall motion, left ventricular volumes are not determined routinely in clinical laboratories due to the additional steps required.

Received Jun. 28, 1991; revision accepted Dec. 4, 1991.

For reprints contact: Wayne C. Levy, MD, Division of Cardiology (111C), Seattle VA Medical Center, 1660 S. Columbian Way, Seattle, WA 98108.

Links et al. (*1*) and Starling et al. (*2*) introduced attenuation-corrected count-based distance methods to determine left ventricular volumes using blood count activity obtained from a blood sample, and an estimate of the distance from the chest wall to the center of the left ventricle, in order to correct for isotope attenuation. Geometric techniques (*4,5*) using methods developed for contrast angiography are simpler to perform but have not received widespread use. Massardo et al. (*3*) recently published a count-based ratio method that does not require attenuation correction or blood sampling.

The original reports by Links, Starling, and Massardo all had very good correlations between radionuclide estimates and contrast angiographic volumes, but the relative accuracies and reproducibilities of these three different manual methods of measuring left ventricular volumes have not been evaluated. All three methods found that manual edge detection was superior to commercially available automated programs. However, manual methods of edge detection have a higher variability (*2*) and are less useful in evaluating serial studies or changes resulting from interventions. It is uncertain if the same manual regions of interest (ROIs) can be used with the count-based distance methods (Links and Starling) and the count-based ratio method of Massardo.

The first purpose of this study was to compare the accuracy and reproducibility of previously described methods of left ventricular volume determination using manual edge detection as described by Links, Starling, and Massardo. In addition, we describe a new count-based ratio method based on the assumption that the ventricle is a prolate ellipse. The second purpose of this study was to determine if left ventricular volume measurements could be successfully automated using an edge detection algorithm developed in our laboratory.

MATERIALS AND METHODS

Patient Selection

We prospectively studied 19 men who were undergoing clinical diagnostic cardiac catheterization and had good quality contrast ventriculograms. Fifteen subjects had significant coronary artery

disease (12 with and 3 without myocardial infarction), 3 had idiopathic dilated cardiomyopathy, and 1 had coronary artery spasm. This study was approved by the Human Subjects Committee of the University of Washington and all patients gave informed consent.

Contrast Ventriculography

Left heart catheterization and coronary arteriography were performed by standard techniques. Following coronary arteriography, contrast ventriculography was performed in the 30° RAO view at 30 frames/sec, using Renograffin 76 or Isovue. Left ventricular volumes were calculated using the single plane area-length method with the Kennedy regression equation (*9*).

Radionuclide Acquisition

Radionuclide angiography was performed 1–3 days following cardiac catheterization in 18 patients and 3 days prior to cardiac catheterization in one patient. No subject had a change in medications or clinical status between studies. Red blood cells were labeled with approximately 1100 MBq ^{99m}Tc using the modified in vivo technique of Callahan et al. (*10*).

All radionuclide angiographic studies were acquired by the same experienced technologist. Imaging was performed in the left anterior oblique (LAO) projection providing the best septal separation of the ventricles with 0–10° of caudal angulation. We acquired 15 million count studies (20 ms/frame) using a GE300 A/M camera with a general all-purpose collimator, a software zoom of 1.5, a 64 × 64 pixel 16-bit word mode image, a 20% energy window, a beat rejection window of ±10% using dynamic arrhythmia filtration (*11*) and a forward/backward reconstruction of the time-activity curve (*12*). Blood sampling and chest imaging, required for the Links (*1*) and the Starling (*2*) methods, were performed as described in the original publications.

Data Processing

Manual Threshold. The images were spatially and temporally smoothed using commercial software (Siemens Microdelta/Maxdelta Imaging System, Des Plaines, IL) prior to manual edge definition. All regions were handdrawn on smoothed unbackground subtracted images by an experienced technologist who was blinded to the angiographic results. A manually drawn region inferior and lateral to the left ventricle was used for background correction. The count data from the hand drawn ROIs were used to calculate left ventricular volumes by the methods as described below. These results will be described as the manual Links, manual Starling, manual Massardo and manual count ratio methods.

Automated Threshold. The images were temporally smoothed using the ¼, ½, ¼ filter and spatially smoothed using a 15 × 15 pixel approximation to a cylindrical Butterworth filter with a frequency parameter of 0.1 cycles/pixel (0.33 cycles/cm) and an order of 4 (*13*). A generous, user-defined, computer-drawn ellipse was placed around the left ventricle on the end-diastolic frame. An interpolative background (*14,15*) illustrated in Figure 1, was calculated for each image. The background constant (V) was calculated by sorting the counts in the pixels on the edge of the end-diastolic image ellipse from the lowest to highest, and averaging the lower one-third of the counts. The background constant (V) is very similar in magnitude to a manually drawn background. The interpolative background was subtracted from the image to isolate the left ventricle. The left ventricular ROI was defined by a 50% threshold of the highest count pixel. The computer-drawn ellipse and the background constant (V) were held constant on all subsequent images for the calculation of the interpolative background. A separate left ventricular ROI was obtained for each image by repeating the above process. These ROIs were then applied to the corresponding unfiltered images to obtain end-diastolic and end-systolic counts. A manually drawn region inferior and lateral to the left ventricle on the unfiltered image was used for background correction. The count data were used to calculate ventricular volumes by the methods described below. These results will be referred to as the automated Links, automated Starling, automated Massardo and automated count ratio methods.

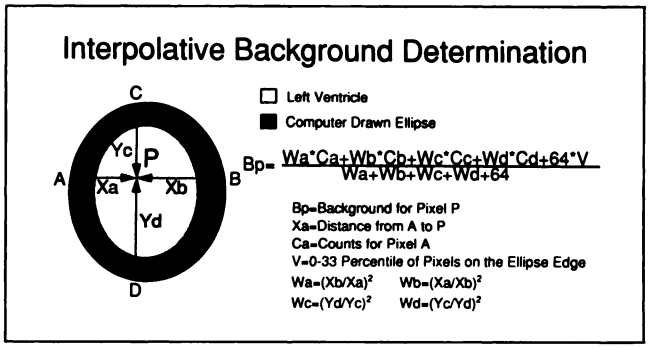

FIGURE 1. A generous user-defined computer-drawn ellipse is placed around the left ventricle on the end-diastolic image. The background constant (V) is calculated on the end-diastolic image by sorting the counts in the pixels on the ellipse edge from the lowest to highest and averaging the counts of the lower one-third (0–33 percentile). The background constant (V) is held constant for all calculations on subsequent images. An interpolative background is calculated for each pixel inside the ellipse for each image with the above formula and is subtracted from the temporally and spatially smoothed images to provide an isolated left ventricle. A 50% count threshold is used to define the ROI. The ROI is then applied to the unfiltered image to obtain end-diastolic and end-systolic counts.

Volume Determination

Links. A ^{57}Co point source was placed over the center of the left ventricle as visually estimated on the camera persistence scope. The camera was then repositioned and an anterior image of the heart was acquired for 60 sec at the 140 ± 10% keV peak for ^{99m}Tc and at the 122 ± 10% keV peak for ^{57}Co. Subsequently, duplicate 3-ml blood samples were positioned 5 cm from the collimator and counted for 5 min. A separate 5-min acquisition without any radioactivity was made to correct for background activity. Ventricular volumes were calculated using previously published formulas (*1*) with the linear attenuation coefficient of water, $\mu = 0.15$ cm^{-1}.

Starling. A mark was placed on the chest wall over the center of the left ventricle in the LAO projection using the persistence scope. A second mark was placed on the chest wall over the center of the left ventricle in the anterior view, defined as halfway between the apex and the aortic valve and the anterior and inferior walls. The horizontal distance between the two marks on the chest wall was measured and used to calculate the distance from the center of the left ventricle to the chest wall. This distance was used in previously published formulas (*2*) to calculate ventricular volumes with the linear attenuation coefficient of water, $\mu = 0.15$ cm^{-1}.

Massardo. The Massardo method (*3*) requires the total counts

in the ROI from the unfiltered image without background subtraction, the average counts of the four highest count pixels in the ROI and the pixel width in cm (M), which varied from 0.294 to 0.302 cm during the study. The counts from the unfiltered end-diastolic frame were applied in the following formula to calculate volumes:

$$\text{Volume} = 1.38\ M^3 \left(\frac{\text{Total counts in ROI}}{\text{Average of 4 highest count pixels}}\right)^{3/2}.$$

The end-systolic volume was calculated from the end-diastolic volume and the ejection fraction.

Count Ratio Method. The Massardo method assumes that the left ventricle can be viewed as a sphere from the appropriate viewing angle (*3,16*). It does not correct for background activity, Compton scatter or for noise in the raw images. The new count ratio method assumes that the ventricle is a prolate ellipse with the major axis 1.8 times the length of the minor axes (*15,16*), uses background correction, corrects for Compton scatter and filters the image with a nine-point spatial smooth to reduce noise prior to the measurement of the highest count pixel. The volume (V_t) is calculated by the formula:

$$V_t = 2.02\ M^3\ C^{3/2} R^{3/2},$$

where M is the width of a pixel (cm), R is the ratio of the total background corrected counts in the ROI divided by the average of the four highest count pixels selected from the filtered background-corrected image and C is the transmission factor of the highest count pixel divided by the transmission factor of the whole ROI. C, which corrects for differences in contribution of Compton scatter in the highest count pixel and the whole ROI, was determined in a 4-cm, 96-ml cylindrical phantom in water and was 1.24 ± 0.01 for the 50% count threshold method and 0.91 ± 0.03 for the manual method. The end-systolic volume (ESV) was calculated from the end-diastolic volume (EDV) and the ejection fraction. The derivation of our method is given in the Appendix.

Reproducibility. To determine interobserver reproducibility, a second technologist analyzed all studies.

Statistical Analysis. The radionuclide methods of volume determination were compared with contrast volumes by means, linear regression, correlation coefficients, and standard error of the estimate (s.e.e.). The coefficient of variation error of the estimate, [CVEE = 100 (s.e.e./mean)], was used to evaluate reproducibility. The Student's t-test was used to compare paired data. To determine if the correlation (precision) between contrast (y) and method 1(r_{1y}) was significantly different from the correlation between contrast and method 2 (r_{2y}), we used the equation (*19*):

$$T = \frac{(r_{1y} - r_{2y})(n-3)^{1/2}}{\left[2(1 - R^2)(1 - r_{12})\right]^{1/2}},$$

where n is the number of observations, r_{12} is the correlation between method 1 and method 2 and R^2 is from the regression model in which contrast is regressed on both method 1 and method 2. The significance of T can then be determined from a table of the t distribution with (n − 3) degrees of freedom. For all comparisons, significance was defined as $p \leq 0.05$.

RESULTS

Volumes

Manual Methods. The results for the four manual methods are shown in Table 1 and Figures 2–3. As the slopes and intercepts for EDV alone and ESV alone were not significantly different for any method, they were combined and are shown as a single plot. The mean contrast ventriculographic volumes (n = 38, 19 EDV and 19 ESV) were 126.6 ml, with a range of 79–292 ml for EDV and 26–225 ml for ESV. The manual Links and Starling methods overestimated the contrast volumes by 50% and 45%, while the manual count ratio method overestimated the contrast volumes by only 12%. The manual Massardo method was superior to the others, as indicated by the accurate mean volume and the lowest s.e.e. Thus, in our laboratory with manual ROI, the Massardo method provided the most accurate volumes. The Starling method was less precise (lower correlation coefficient) than the Links, Massardo and the count ratio method (all $p < 0.05$). There was no significant difference in precision between the other methods.

TABLE 1
Comparison of Manual Radionuclide Volumes and Contrast Volumes

	Mean (ml)	r	Slope	Intercept	s.e.e.
Contrast angiography	126.6				
Manual Links	189.7†	0.85‡	1.24	32.8	49.0
Manual Starling	183.2†	0.77	1.12	41.4	58.3
Manual Massardo	122.5	0.91‡	0.95	2.2	26.3
Manual count ratio	141.4*	0.90‡	1.13	−1.4	34.5

* $p < 0.01$ vs. contrast, † $p < 0.0001$ vs. contrast, ‡ $p < 0.05$ vs. Starling.
r = correlation coefficient.

Automated Methods. The volumes obtained using the automated algorithm for each method are shown in Table 2 and Figures 2 and 4. The automated Links,

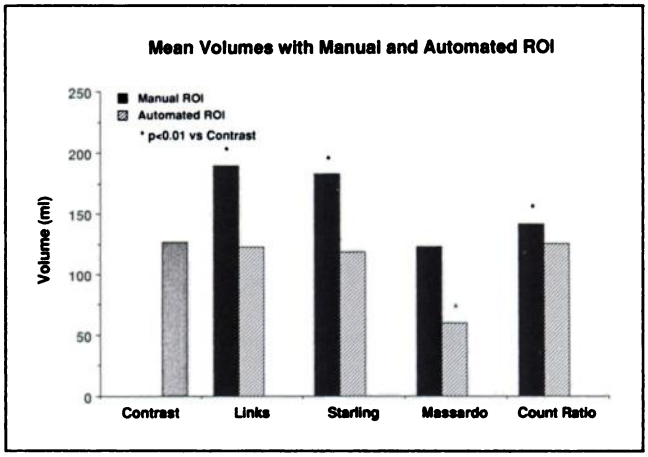

FIGURE 2. The mean volumes obtained using manual and automated ROIs with the four different radionuclide methods are compared with contrast volumes.

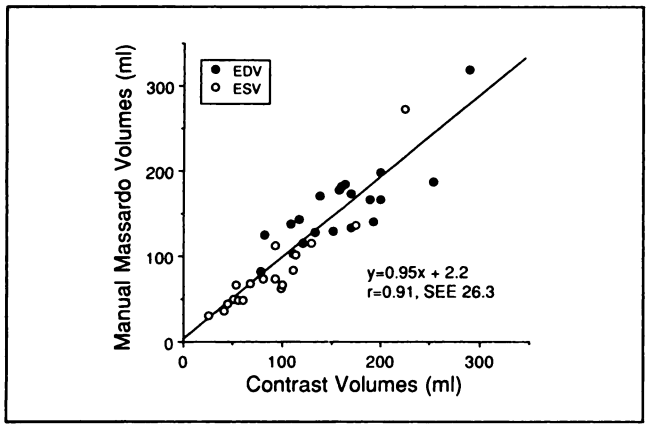

FIGURE 3. Contrast volumes are compared with radionuclide volumes obtained with the Massardo method using manual ROIs.

Starling and count ratio methods all provided accurate volumes, while the automated Massardo method underestimated the contrast volumes by 53%. The automated count ratio method and the automated Links method were comparable, as indicated by a similar correlation coefficient and s.e.e. Both methods had a lower s.e.e. and a higher correlation coefficient than the automated Starling method. The Starling method was less precise than the Links, Massardo and the count ratio method (all $p < 0.05$). There was no significant difference in precision between the other methods.

Ejection Fraction. The mean ejection fraction was 46.4 (range = 23–67) for contrast angiography, 49.6 for the automated technique, and 50.7 for the manual technique. The manual and the automated ejection fractions had similar correlation coefficients and s.e.e. (Table 3).

Reproducibility. The reproducibilities of the manual and automated methods are shown in Table 4. The mean differences between observer 1 and observer 2 was less for the automated methods (2–5 ml, 1.3%–3.9%) than the manual methods (3–14 ml, 2.2%–7.6%). Additionally, the interobserver CVEE was also less for the automated methods (7.5%–8.4%) compared to the manual methods (9.1%–10.5%). The reproducibilities for the Links and the Starling methods underestimates the true reproducibilities since they do not include the additional variability that would be introduced by resampling and recounting the blood radioactivity or remeasuring the distance to the center of the left ventricle.

The interobserver reproducibility of the automated ejection fraction was excellent with a mean difference of −0.4 EF units and a CVEE of 4%. This was less than the manual

TABLE 2
Comparison of Automated Radionuclide Volumes and Contrast Volumes

	Mean (ml)	r	Slope	Intercept	s.e.e.
Contrast angiography	126.6				
Automated Links	122.4	0.89‡	0.90	7.9	29.8
Automated Starling	118.1	0.81	0.81	14.9	36.4
Automated Massardo	59.5†	0.90‡	0.48	−0.9	14.2
Automated count ratio	125.0	0.90‡	1.02	−3.6	31.4

† $p < 0.0001$ vs. contrast, ‡ $p < 0.05$ vs. Starling.
Abbreviations as in Table 1.

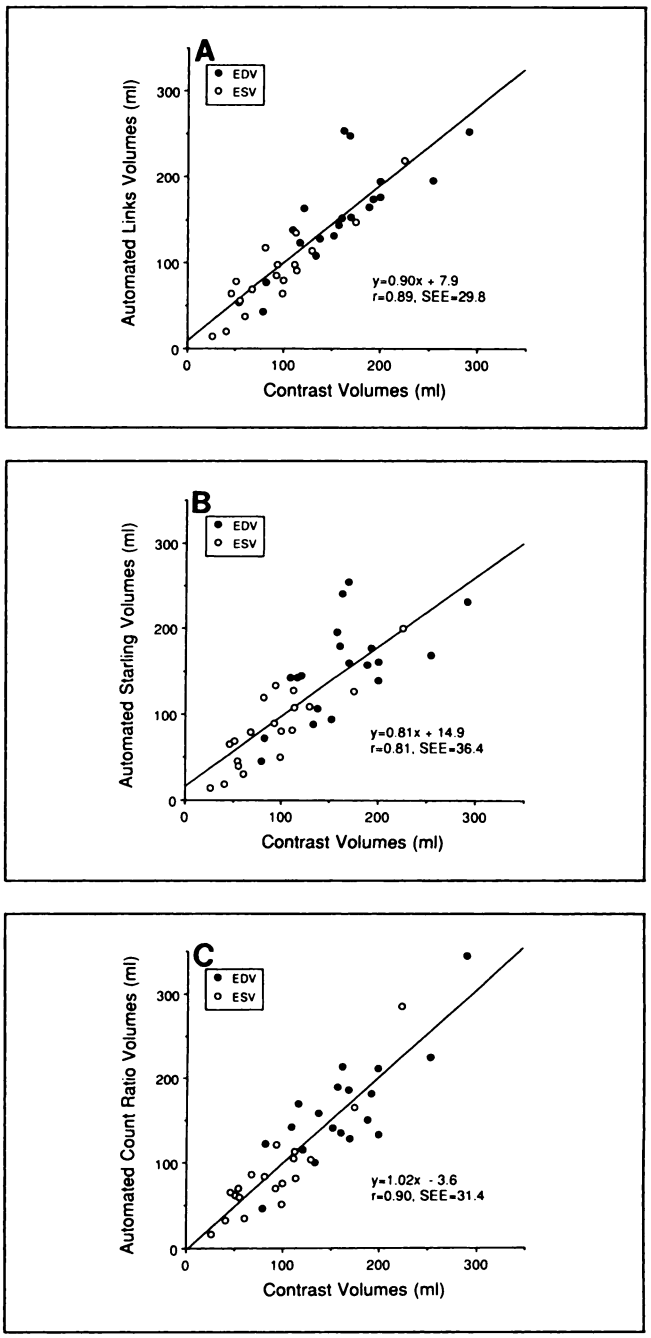

FIGURE 4. Contrast volumes are compared with radionuclide volumes obtained using automated ROIs with: (A) the Links method, (B) the Starling method and (C) the count-ratio method.

TABLE 3
Comparison of Radionuclide and Contrast Ejection Fractions

	Mean (ml)	r	s.e.e.
Contrast	46.4		
Manual	50.7	0.85	8.1
Automated	49.6	0.80	9.4

Abbreviations as in Table 1.

interobserver reproducibility (mean difference −0.8 EF units and CVEE of 6.0%).

DISCUSSION

The prognostic importance of ejection fraction and left ventricular volumes, especially ESV, have been well established in patients with a wide variety of heart disorders (*20–24*). The ability to accurately measure cardiac volumes is useful, but due to time constraints, it is generally not employed in routine clinical nuclear cardiology laboratories. The automated count ratio method described in this report requires no additional images, blood counts or attenuation correction for the determination of cardiac volumes, and thus can be applied in the clinical laboratory for the measurement of both ejection fraction and cardiac volumes. The total processing time to measure ejection fraction and cardiac volumes is approximately 10 min. The processing time could be substantially shorter if only end-diastolic and end-systolic ROIs were used, rather than separate ROIs for each 20 msec image.

TABLE 4
Interobserver Reproducibility

Manual volumes (ml)	Mean difference (ml)	r	CVEE
Links*	−14.4 (−7.6%)	0.98	10.5%
Starling*	−13.4 (−7.3%)	0.98	10.7%
Massardo	−2.7 (−2.2%)	0.99	9.1%
Count ratio	−7.6 (−5.4%)	0.99	9.7%
Automated Volumes (ml)	**Mean difference (ml)**	**r**	**CVEE**
Links*	1.6 (1.3%)	0.99	7.9%
Starling*	1.8 (1.5%)	0.99	8.4%
Massardo	2.3 (3.9%)	0.99	8.1%
Count ratio	4.8 (3.8%)	0.99	7.5%
Ejection Fraction	**Mean difference**	**r**	**CVEE**
Manual	−0.8	0.98	6.0%
Automated	−0.4	0.99	4.0%

r = correlation coefficient and CVEE = coefficient of variation error of the estimate.

* Reproducibility testing for the Links and the Starling methods did not include repeat measures of the blood radioactivity or the distance to the center of the left ventricle. Inclusion of these factors would result in additional variability.

Manual Methods

In a direct comparison of four different methods of left ventricular volume determination using manual ROIs, only the Massardo method provided accurate volumes compared to contrast angiography. We thus confirmed the accuracy and reproducibility of the initial report of Massardo using manual ROIs. Thus, although Links, Starling and Massardo all used manual ROIs in their original reports, we have shown that the same manual ROIs cannot be used with these different methods.

The use of an attenuation coefficient of 0.15 cm^{-1} with a manual ROI, as originally described by Links and Starling, resulted in mean volumes that were 45%–50% too large in the current study. This overestimation was probably due to inclusion of Compton-scattered photons in the ROI. The manual ROI identified an area significantly larger than the left ventricular cavity. Links used an in vivo RBC labeling technique and Starling used ^{99m}Tc-labeled albumin. Both of these methods result in a higher background activity (and thus greater background subtraction) than the modified RBC labeling technique (*25*) that we utilized. Thus, in the original reports, the effects of Compton scatter may have been compensated for by oversubtracting the background activity.

Automated Methods

We have developed an automated edge detection algorithm based on Butterworth filtering, an interpolative background subtraction and a 50% count threshold-based ROI. This new automated method was successfully applied to the Links, Starling and a new count ratio method to provide automated volume determinations. Prior attempts to automate cardiac volume measurement using a commercial second derivative algorithm have resulted in the following underestimation of contrast volumes: 41% by Links (*1*), 15% by Starling (*2*) and 22% by Massardo (*3*). In comparison, our results using an interpolative background algorithm with a 50% count threshold yielded accurate volumes for the following three methods; −3% for Links, −7% for Starling, and −1% for the count ratio method. However, the automated method significantly underestimated volumes with the Massardo method (−53%).

The automated ROI was 49% smaller than the manual ROI, presumably excluding many scattered photons. The automated ROI did not differ significantly from left ventricular dimensions estimated by echocardiography in 10 patients (data not shown).

The accuracy and precision of the automated Links and the automated count ratio method are similar. The Starling method was less precise than the other three methods, for both the manual and the automated ROIs. A major strength of the automated method is the high reproducibility which is optimal for serial studies in a given subject.

Comparison

The automated method provides precision comparable to the original reports as estimated by s.e.e. for EDV and ESV combined (current versus original) for the Links (s.e.e. = 30 versus 34 ml) and Starling methods (s.e.e. = 36 versus 27 ml) (*26*). The Massardo manual method provided similar precision as the original report by Massardo (s.e.e. = 26 versus 23 ml). The correlation coefficients are lower in the current report due to a smaller range of volumes than were present in the original reports of Links and Starling.

Butterworth filtering provides a very smooth image which is necessary for applying this method to low count studies (i.e., exercise), but for routine higher count clinical studies (i.e., 4 million frame mode), conventional temporal and spatial smoothing is adequate (data not shown). The Links, Starling, and the count ratio methods are also valid with low count studies, but the highest count pixel for the count ratio method must be selected from the Butterworth filtered image because the nine-point smooth does not adequately reduce the noise in these studies (data not shown). The interpolative background subtraction is the unique characteristic which allows excellent septal, aortic, and atrial separation. Although manual override of the automated ROI is possible when applying the count threshold, this was necessary in only one patient where inadequate ventricular separation from the atria occurred at end-systole. Because this method requires only a single ellipse at end-diastole to obtain an individual ROI for each image, it should be applicable to diastolic function analysis, radionuclide pressure volume loop analysis, as well as determination of ventricular volumes and ejection fractions.

Method Limitations

All four methods are sensitive to variations in the ROI. Count-based ratio methods, i.e., Massardo and the new count ratio method, are influenced by the viewing angle of the ventricle (*16*) and noise in the image, because this influences the highest count pixel. Both count-based ratio methods would be expected to overestimate ventricular volumes if the heart is imaged perpendicular to the long-axis (i.e., vertical hearts) rather than a usual 40–50° viewing angle (*16*). The new count ratio method reduces the variability due to noise by spatial smoothing, but introduces background subtraction variability and a constant derived from phantoms to correct for the inclusion of Compton scatter photons that varies between different methods used to define the ROI and may vary between different gamma cameras. The count-based ratio method may tend to overestimate cardiac volumes in severely dilated ventricles (EDV > 350 ml) as the length to diameter ratio approaches 1.4–1.6:1 rather than the 1.8:1 in ventricles <300 ml (*17, 18*). Because we had no contrast volumes greater than 300 ml, we were unable to test this.

On the other hand, count-based distance methods, i.e., Links and Starling, are subject to variations in background subtraction and assume uniform attenuation within and between subjects. Most importantly, however, the count-based distance methods of Links and Starling require an accurate estimate of the distance from the chest wall to the center of the left ventricle as well as accurate blood sampling. Both of these steps would introduce additional variability, which was not measured in this study. Thus, our estimates of the interobserver reproducibility of the Links and Starling methods almost certainly underestimates their total variability if repeat blood sampling and determination of the distance to the center of the left ventricle were included.

Study Limitations

The 50% threshold was determined retrospectively. We used a single estimate of the distance from the chest wall to the center of the left ventricle as did Links, while Starling used the average of six measurements (three measurements by two different observers). Finally, contrast ventriculography is used as a reference method because of the validation performed in post mortem studies with AP-lateral biplane angiocardiograms (*27*). However, it is influenced by geometric assumptions, prior contrast load, fluctuating hemodynamics and represents a single contraction. The interobserver variability for contrast ventriculography is 5.9% ± 3.4% for EDV, 8.0% ± 2.3% for ESV and 5.3% ± 1.5% for ejection fraction in our reference laboratory (*28*). The contrast ventriculographic variability is similar to the 7.0% for EDV, 8.9% for ESV and 4.0% for ejection fraction for with the automated algorithm used in this radionuclide study.

CONCLUSION

We have developed an automated edge detection algorithm to determine absolute left ventricular volumes with the Links, Starling, and our own count ratio method. Our automated count ratio method is as accurate, precise and reproducible as earlier methods, but requires no additional images, blood counts, attenuation or decay correction. The count ratio method could readily be incorporated into routine clinical laboratory use.

APPENDIX

Derivation of the Count-Based Ratio Method for Volume Determination

The following derivation is based on the original derivation by Massardo et al. (*3*). The count proportional volume theory states that the total number of gamma rays that pass through a collimator (total counts) is proportional to the total volume independent of its shape. The maximum pixel count for a uniform activity distribution is proportional to an effective reference volume defined as the product of the length of the longest axis perpendicular to the collimator and the cross-sectional area of the pixel. The left ventricle can be represented by a prolate ellipse with the major axis 1.8 times the minor axes for left

ventricular volumes <300 ml (*17,18*). If we assume the left ventricle is a prolate ellipse and the major axis is 1.8 times the minor axis (length of major axis = 1.8 × minor axis (D)), and the minor axes are equal, the volume of the prolate ellipse (V_t) is:

$$V_t = (\pi/6)(D)(D)(1.8D) = 0.3\ \pi D^3. \quad \text{Eq. 1}$$

The reference volume (V_r) is defined as the cross-sectional area of a pixel (M is the pixel width in cm), multiplied by its length (L), $V_r = LM^2$. Since the highest count pixel is used, the reference volume length (L) is the longest length of the left ventricle perpendicular to the gamma camera. The reference volume length in the LAO projection is intermediate between the major and the minor axis of the left ventricle (*3,16*) and roughly corresponds to a line drawn from the distal anterior wall to the base of the mitral valve. We measured the reference volume length in 38 contrast ventriculograms at end-diastole and end-systole. The reference volume length is 0.87 ± 0.09 times the length of the major axis. The reference volume length is thus L = 0.87 × length of the major axis = 0.87 × 1.8D = 1.57D, where D = the minor axis. The counts in the highest count pixel (N_m) equals the counts/cm^3 of blood (k) multiplied by the reference volume (LM^2) and by the transmission factor for the highest count pixel (TF_m):

$$N_m = kV_rTF_m = kLM^2TF_m = 1.57kDM^2TFm. \quad \text{Eq. 2}$$

The total counts (T_c) in the left ventricle equals the counts/ml of blood (k) multiplied by the volume of the left ventricle (V_t) and by the transmission factor for the ROI used to define the total counts in the left ventricle (TF_t):

$$T_c = kV_tTF_t = 0.3\ k\pi D^3TF_t. \quad \text{Eq. 3}$$

The counts/ml of blood (k) is eliminated by taking the ratio $R = T_c/N_m$ and combining Equations 2 and 3. The ratio R is equal to the number of reference volumes in the prolate ellipse:

$$R = \frac{T_c}{N_m} = \frac{0.3\ k\pi D^3TF_t}{1.57kDM^2TF_m} = \frac{D^2TF_t}{1.66M^2TF_m}. \quad \text{Eq. 4}$$

Although the absolute transmission factors decreases with distance, the ratio TF_m/TF_t does not vary over depths of 5–15 cm. In ideal imaging, without point spread functions and Compton scatter, the ratio would be unity (*1*), but due to the broad photopeaks employed in nuclear medicine there is a considerable contribution of Compton-scattered photons to the counts detected in the highest count pixel and in the whole ROI. The ratio TF_m/TF_t is relatively constant (C) for each method used to define the ROI but will vary for different methods used to define the ROI (i.e., 50% count threshold versus manual). Solving Equation 4 for D and substituting $C = TF_m/TF_t$ yields:

$$D = (1.66M^2RC)^{1/2}. \quad \text{Eq. 5}$$

The volume of a prolate ellipse (V_t) is given by substituting Equation 5 into 1:

$$V_t = 0.3\pi D^3 = 0.3\pi(1.66M^2RC)^{3/2} \quad \text{Eq. 6}$$

or

$$V_t = 2.02\ M^3C^{3/2}R^{3/2}, \quad \text{Eq. 7}$$

where M is the width of a pixel (cm) determined for each pixel matrix and R is the ratio of the total background corrected counts in the ROI divided by the average of the four highest count pixels selected from the filtered background-corrected image. C was determined in a 4-cm, 96-ml cylindrical phantom in water at depths of 5–15 cm (1.2–2.4 cm increments) for each method used to define the ROI. For a 50% count threshold ROI, C = 1.24 ± 0.01 and for the manual ROI C = 0.91 ± 0.03.

ACKNOWLEDGMENTS

We would like to thank the cardiac catheterization laboratory personnel, the reference volume laboratory personnel, and John Martin for his assistance in the analysis of the radionuclide ventriculograms. We also thank Arnold F. Jacobson, MD, PhD and James Ritchie, MD for their critical reviews of the manuscript, and Jim Kousbaugh for his assistance in preparing the manuscript.

Supported by the Research Service of the Department of Veterans Affairs, Washington, DC, NIH grant AG 06581, and the Dana Foundation, New York, NY.

REFERENCES

1. Links JM, Becker LC, Shindledecker JG, et al. Measurement of absolute left ventricular volume from gated blood-pool studies. *Circulation* 1982;65:82–90.
2. Starling MR, Dell'Italia LJ, Walsh RA, Little WC, Benedetto AR, Nusynowitz ML. Accurate estimates of absolute left ventricular volumes from equilibrium radionuclide angiographic count data using a simple geometric attenuation correction. *J Am Coll Cardiol* 1984;3:789–798.
3. Massardo T, Gal RA, Grenier RP, Schmidt DH, Port SC. Left ventricular volume calculation using a count-based ratio method applied to multigated radionuclide angiography. *J Nucl Med* 1990;31:450–456 and *J Nucl Med* 1990;31:1449 [correction].
4. Massie BM, Kramer BL, Gertz EW, Henderson SG. Radionuclide measurement of left ventricular volume: comparison of geometric and counts-based methods. *Circulation* 1982;65:725–730.
5. Seldin DW, Esser PD, Nichols AB, Ratner SJ, Alderson PO. Left ventricular volume determined from scintigraphy and digital angiography by a semi-automated geometric method. *Radiology* 1983;149:809–813.
6. Stadius ML, Williams DL, Harp G, et al. Left ventricular volume determination using single-photon emission computed tomography. *Am J Cardiol* 1985;55:1185–1191.
7. Caputo GR, Graham MM, Brust KD, Kennedy JW, Nelp WB. Measurement of left ventricular volume using single-photon emission computed tomography. *Am J Cardiol* 1985;56:781–786.
8. Bunker SR, Hartshorne MF, Schmidt WP, et al. Left ventricular volume determination from single-photon emission computed tomography. *AJR* 1985;144:295–298.
9. Kennedy JW, Trenholme SE, Kasser IS. Left ventricular volume and mass from single-plane cineangiocardiogram. A comparison of anteroposterior and right anterior oblique methods. *Am Heart J* 1970;80:343–352.
10. Callahan RJ, Froelick JW, McKusick KA, Leppo J, Strauss HW. A modified method for the in vivo labeling of red blood cells with Tc-99m: concise communication. *J Nucl Med* 1982;23:315–318.
11. Wallis JW, Wu-Connolly L, Rocchini AP, Juni JE. Dynamic arrhythmia filtration for gated blood-pool imaging: validation against list mode technique. *J Nucl Med* 1986;27:1347–1352.

12. Cerqueira MD, Harp GD, Ritchie JL, Stratton JR, Walker RD. Rarity of preclinical alcoholic cardiomyopathy in chronic alcoholics <40 years of age. *Am J Cardiol* 1991;67:183–187.
13. Budinger TF, Gullberg GT, Huesman RH. *Topics in applied physics: image reconstruction from projections, volume 32.* New York: Springer-Verlag; 1979:197–199.
14. Sinusas AJ, Beller GA, Smith WH, Vinson EL, Brookeman V, Watson DD. Quantitative planar imaging with technetium-99m-methoxyisobutyl isonitile: comparison of uptake patterns with thallium-201. *J Nucl Med* 1989;30:1456–1463.
15. Koster K, Wackers FJT, Mattera JA, Fetterman RC. Quantitative analysis of planar technetium-99m-sestamibi myocardial perfusion images using modified background subtraction. *J Nucl Med* 1990;31:1400–1408.
16. Grenier R, Port S. Geometric methods for determining left ventricular volume [Reply]. *J Nucl Med* 1991;32:553–555.
17. Sandler H, Dodge HT. The use of single plane angiocardiograms for the calculation of left ventricular volume in man. *Am Heart J* 1968;75:325–334.
18. Laskey WK, John Sutton M, Zeevi G, Hirshfeld JW, Reichek N. Left ventricular mechanics in dilated cardiomyopathy. *Am J Cardiol* 1984;54:620–625.
18. Hotelling H. The selection of variates for use in prediction with some comments on the general problem of nuisance parameters. *Ann Math Stat* 1940;11:271–283.
20. Moss AJ, et al. Risk stratification and survival after myocardial infarction. *N Engl J Med* 1983;309:331–336.
21. Lee LL, Pryor DB, Pieper KS, et al. Prognostic value of radionuclide angiography in medically treated patients with coronary artery disease. *Circulation* 1990;82:1705–1717.
22. White HD, Norris RM, Brown MA, et al. Left ventricular end-systolic volume is the major determinant of survival after recovery from myocardial infarction. *Circulation* 1987;76:44–51.
23. Henry WL, Bonow RO, Borer JS, et al. Observations on the optimum time for operative intervention for aortic regurgitation. I. Evaluation of the results of aortic valve replacement in symptomatic patients. *Circulation* 1980;61:471–483.
24. Henry WL, Bonow RO, Rosing DR, Epstein SE. Observations on the optimum time for operative intervention for aortic regurgitation. II. Serial echocardiographic evaluation of asymptomatic patients. *Circulation* 1980;61:484–492.
25. Neumann P, Schicha H, Schurnbrand P, Bahre M, Emrich D. Visualizing cardiac blood pool: comparison of three labeling methods. *Eur J Nucl Med* 1983;8:463–466.
26. Starling MR, J Dell'Italia LJ, Nusynowitz ML, Walsh RA, Little WC, Benedetto AR. Estimates of left-ventricular volumes by equilibrium radionuclide angiography: importance of attenuation correction. *J Nucl Med* 1984;25:14–20.
27. Dodge HT, Sandler H, Ballew DW, Lord JD. The use of biplane angiocardiography for the measurement of left ventricular volume in man. *Am Heart J* 1960;60:762–776.
28. Sheehan FH, Mitten-Lewis S. Factors influencing accuracy in left ventricular volume determination. *Am J Cardiol* 1989;64:661–664.

(continued from page 747)

SELF-STUDY TEST
Skeletal Nuclear Medicine

ANSWERS

5. Lavender JP, Khan RAA, Hughes SPF. Blood flow and tracer uptake in normal and abnormal canine bone: comparison with Sr-85 microspheres, Kr-81m, and Tc-99m MDP. *J Nucl Med* 1979;20:413–418.
6. McInnis JC, Robb RA, Kelly PJ. The relationship of bone blood flow, bone tracer deposition, and endosteal new bone formation. *J Lab Clin Med* 1980;96:511–522.
7. Siegel BA, Donovan RL, Alderson PO, Mack GR. Skeletal uptake of ^{99m}Tc-diphosphonate in relation to local bone blood flow. *Radiology* 1976;120:121–123.
8. Vattimo A, Martini G, Pisani M. Bone uptake of ^{99m}Tc-MDP in man: its relationship with local blood flow. *J Nucl Med Allied Sci* 1982;26:173–179.

ITEM 3: Interpretation of Lumbar Bone Mineral Measurements

ANSWER: E

When significant degenerative hypertrophic changes are present, or when markedly calcified plaques in the aorta overlie the spine, the measured bone mineral does not accurately reflect bone density in the vertebrae alone and cannot be used to draw diagnostic conclusions regarding bone mass or fracture risk. Other conditions interfering with measurement of spinal bone mass are listed in Table 1. Most of the time, these can be identified from the spinal radiographs obtained before the test. Occasionally, however, these problems first become apparent when the bone mineral image is being reviewed.

The tracing depicted in Figure 1 is of good quality and shows no evidence of degenerative disease, spinal deformity, artifacts, or technical problems. There is a uniform distribution of bone mineral in this patient's lumbar spine.

Although the bone mineral images occasionally show bone mineral in the region of the transverse processes on some types of instruments, the processing algorithm eliminates these areas. Further, a manual override is available to allow checking and correcting of the edges if necessary. The image can be displayed with the edges identified for final assessment. In this patient, this would not be necessary.

Less than half of all women with bone mineral values of 0.75 g/cm^2 have a spinal compression fracture (Table 2). This statistic stresses the distinction between the assessment of fracture risk by bone mineral measurements and the diagnosis of fracture or other irreversible changes by radiography.

Bone mineral assessment is the only nontraumatic test that can be used to measure bone mass in patients at high risk of bone loss prior to the occurrence of irreversible changes. Also, in patients with compression fractures, the amount of bone mass actually present and the risk for further fractures can be assessed only by bone mineral meas-

TABLE 1
False Results in Bone Mineral Measurements

Conditions resulting in falsely high bone mineral	Conditions resulting in falsely high or low bone mineral
Marked aortic calcification	Compression fractures and other post traumatic changes
Hypertrophic degenerative joint and disc disease	Marked scoliosis and other spinal deformities
Bone grafts	Focal vertebral lesions (lytic or sclerotic)
Lipiodol in the spinal canal	
Calcium-containing tablets in the gastrointestinal tract	
Conditions resulting in falsely low bone mineral	
Laminectomy	

[Table 1 adapted from Freeman LM, Weissmann HS, eds, *Nuclear Medicine Annual 1986.* Raven Press, 1986:195–226.]

TABLE 2
Relationship Between Bone Mineral and Fracture Risk in Normal Women from Minnesota

Bone mineral in spine or femur (g/cm^2)	Prevalence of L1–L4 vertebral fractures (%)	Proximal femoral fracture incidence per 1000 person-years	
		Neck	Trochanter
>1.40	0	0	0
1.20–1.39	0.1	0	0
1.00–1.19	6.8	0.2	0.1
0.80–0.99	26.1	2.0	0.8
0.60–0.79	47.5	6.5	5.3
<0.60	48.8	8.8	17.6

[Table 2 adapted from Wahner HW. Single- and dual-photon absorptiometry in osteoporosis and osteomalacia. *Semin Nucl Med* 1987;17:305–315.]

(continued on page 776)